

IA-TIGRIS: An Incremental and Adaptive Sampling-Based Planner for Online Informative Path Planning

Brady Moon¹, Nayana Suvarna¹, Andrew Jong¹, Satrajit Chatterjee², Junbin Yuan³, and Sebastian Scherer¹

Abstract—Planning paths that maximize information gain for robotic platforms has wide-ranging applications and significant potential impact. To effectively adapt to real-time data collection, informative path planning must be computed online and be responsive to new observations. In this work, we present IA-TIGRIS, an incremental and adaptive sampling-based informative path planner that can be run efficiently with onboard computation. Our approach leverages past planning efforts through incremental refinement while continuously adapting to updated world beliefs. We additionally present detailed implementation and optimization insights to facilitate real-world deployment, along with an array of reward functions tailored to specific missions and behaviors. Extensive simulation results demonstrate IA-TIGRIS generates higher-quality paths compared to baseline methods. We validate our planner on two distinct hardware platforms: a hexarotor UAV and a fixed-wing UAV, each having unique motion models and configuration spaces. Our results show up to a 41% improvement in information gain compared to baseline methods, suggesting significant potential for deployment in real-world applications. Project website and video at ia-tigris.github.io.

Index Terms—Aerial Systems: Perception and Autonomy, Motion and Path Planning, Reactive and Sensor-Based Planning, Field Robots

I. INTRODUCTION

Robots play a vital role in gathering information from the physical world, supporting a wide range of applications such as scientific research [1]–[3], environmental monitoring [4]–[8], search and rescue operations [9], [10], and disaster response efforts [11]–[13]. By employing intelligent algorithms, robotic systems enhance the efficiency of data collection, provide valuable insights, and support well-informed decision-making processes. These autonomous robots provide unparalleled advantages in situations where human access is constrained, dangerous, or logistically challenging [14]. Moreover, the scalability and speed of autonomous information gathering robots significantly enhances the rate of information gathering by not capping the number of robots based on the number of human operators.

This work is supported by the Office of Naval Research (Grant N00014-21-1-2110). This material is based upon work supported by the National Science Foundation Graduate Research Fellowship under Grant No. DGE1745016.

¹Authors are with the Robotics Institute, School of Computer Science at Carnegie Mellon University, Pittsburgh, PA, USA {bradym, nsuvarna, ajong, basti}@andrew.cmu.edu

²Author is with the GRASP Lab at the University of Pennsylvania, Philadelphia, PA, USA satrajit@seas.upenn.edu

³Author is with the Mechanical Engineering Department at Carnegie Mellon University, Pittsburgh, PA, USA junbiny@andrew.cmu.edu

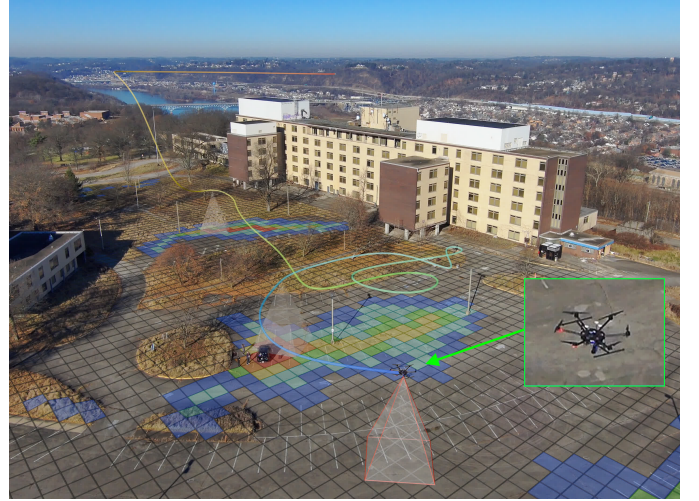


Fig. 1. IA-TIGRIS deployed on a hexarotor UAV to map the location of cars in the environment. The visualization shows a probability grid representing the prior belief of car locations and a representative path generated by our planner. The algorithm runs entirely onboard, continuously refining and adapting paths based on updated world beliefs from sensor observations.

Informative path planning (IPP) seeks to create intelligent paths for robots to execute actions that maximize their inherent potential and advantages in data gathering situations, while not violating budget constraints on the system or mission. This approach has many advantages over most coverage-based approaches which often don’t take into account the flight time of the drone or prior information about the space and don’t adapt to learned information during flight. However, solving the IPP problem is computationally expensive, being at least NP-hard even in a discrete space [15], leading to methods that only plan over a short horizon or are static during the path execution.

In this work, we introduce IA-TIGRIS (Incremental and Adaptive Tree-based Information Gathering using Informed Sampling), a sampling-based informative path planner that incrementally builds its search tree and adapts to new information online by efficiently updating and building the set of possible trajectories. This leads to global paths that are more robust to path execution disturbances, adapt to changes in the information map, and are higher quality than a single plan due to continual online refinement. Fig. 1 demonstrates IA-TIGRIS deployed on a hexarotor drone for an IPP application. Our key contributions are the following:

- A novel incremental and adaptive sampling-based planner

for IPP that dynamically plans online using the updated belief map. We provide key implementation details, insights, and optimizations that enable efficient trajectory evaluation and updates during incremental planning.

- Thorough testing and evaluation of our method against other baselines, as well as ablations and analysis on the components of our algorithm.
- Hardware validation on two distinct UAV platforms with different motion constraints and configuration spaces, demonstrating versatility and real-world applicability.

The paper is organized as follows: Section II gives a detailed overview of related works and the contributions of this work. Section III presents the problem formulation. Our proposed approach is detailed in Section IV. The section outlines the planner’s design and its integration with system components to enable adaptive and efficient informative path planning for real-world applications. Section V provides our detailed experimental evaluation and results of the approach. The results of our field deployments are summarized in Section VI, and Section VII offers the conclusion and future work.

II. RELATED WORKS

One way to formulate the IPP problem is to discretize the continuous space into a fixed set of states. Many previous works have then used this discrete space to view IPP as an orienteering problem. Given a weighted-undirected graph, orienteering involves determining a Hamiltonian path over a subset of nodes with the objective of maximizing the total reward while subject to a constraint on the path cost. The orienteering problem can be thus broken down into an optimization objective that involves selecting a subset of nodes from the given graph and a traveling salesman problem, that aims to minimize the distance traveled while visiting the selected subset of nodes. This optimization objective, which dictates how the subset of nodes are selected, can be chosen based on the specific task to which orienteering is being applied. For example [16] applies it to the task of environmental monitoring in an aquatic setting while [17] applies it to the more general Constraint Satisfaction Problem (CSP).

However, framing IPP as an orienteering problem leads to computationally expensive runtimes, which rapidly become intractable as the likelihood of near-optimal paths in the solution space diminishes. As the authors [18] note, the IPP problem is a NP-hard search problem. In order to overcome this, the authors develop an approximation algorithm that efficiently finds near-optimal solutions leveraging mutual information in the problem space. They do this by ensuring that the mutual information formulation is submodular in nature as discussed in [19]. This results in a diminishing returns property whereby making a new observation yields more information if fewer observations have been made up to that point, and less information if many observations have already been made. Hence, the IPP problem can be reformulated as maximizing a submodular objective function while constrained to a budget. [20] studies this formulation by developing a recursive-greedy algorithm that they show has strong theoretical guarantees.

However, these mentioned approaches have only been used in applications that have relatively small search spaces such

as environmental monitoring [16], water quality monitoring and analysis [21], or detection of chemical or biological plumes [22] that are then discretized into a finite set of sensing locations. As one can imagine, this becomes quickly intractable in applications that have much larger search spaces, are higher dimensional, or both. Examples of this type of situation include searching for targets of interest over a large search area, such as a missing hiker or tracking multiple dynamic targets of interest over a larger search area, such as ships at sea. In order to combat this, the authors in [16] propose using heuristics while [16], [20], [23] also suggest using greedy approaches to approximate solutions. Another method involves Mixed Integer Programming (MIP) based solutions such as [24]. But these solutions fail to capture the relationship between nodes which would not be ideal for many problem statements. The limitations in capturing the relationship in rewards among nodes along with the inefficient run times necessitate developing better exploration algorithms that would allow for robust information gathering by autonomous systems in complex problem settings.

Some previous approaches have tried using receding horizon-based methods to solve the IPP problem. Local receding-horizon based solutions optimize the information-objective over a small lookahead or horizon. They rely on replanning to approach a globally optimal solution. One such approach involves a receding horizon algorithm [25] that satisfies a temporal logic specification for problem statements where safety and reliability are paramount. Another approach by [26] involves using a receding horizon planner to perform informative planning in a latent environment modeled using Gaussian processes. According to [27], receding horizon-based path planners are susceptible to becoming trapped in local optima. To address this issue, the study explores the impact of adjusting the horizon length and considers adapting it based on the remaining information. They propose a J-Horizon algorithm, which incorporates a lookahead step size to improve convergence toward better optima. Despite these improvements, receding horizon methods primarily plan optimal paths reactively and fail to fully utilize the available prior information about the environment [28].

Notably, [29] compares lawnmower paths with other planning algorithms and observes that their performance is only slightly inferior to that of adaptive algorithms. Furthermore, the study concludes that graph-based search algorithms underperform compared to lawnmower patterns due to their limited ability to adapt to uncertainties in prior information. The ability to allow for revisits is very important for finding globally optimal paths, especially when the information objective is submodular or when the task requires revisits [30]. Another approach which has shown promise involves branch and bound techniques which prune suboptimal branches early in the tree search [31], [32]. However, efficiently calculating tight bounds in problems with unknown environments and high-dimensional state space is nontrivial. Previous works have solved this using Gaussian processes (GP). However, implementing GPs is application specific and a specific approach used in one work may not be transferable to another application. Secondly, the computational complexity of inference in

GPs generally scale cubically with the number of observations [33]. Although methods exist to mitigate this complexity, long-horizon planning remains computationally demanding unless stationary assumptions are made about the covariance function. This is further compounded when planning in higher-dimensional state spaces.

Numerous works have worked to address these drawbacks by formulating the task of information gathering in continuous space and introducing adaptive sampling-based algorithms. Examples of some of these works include [34], [35], [36]–[41]. These methods employ sampling-based approaches, which involves the selection and inclusion of new states in continuous space into a tree structure. As the tree grows, the optimal path—maximizing information gain while respecting budget constraints—is continuously refined and the best path is selected. However, these approaches face significant challenges in expansive spaces, where increasing dimensionality causes the search space to grow substantially relative to regions of high information reward. In order to address these challenges, [30] introduced a sampling-based approach for IPP in large and high-dimensional search spaces. The method performs informed sampling within the continuous space and incorporates edge information gain during reward estimation, efficiently generating global paths that optimize information gathering within budget constraints.

While [30] demonstrated effective global planning, the approach generated static plans that remained unchanged during robot execution. Our proposed algorithm, IA-TIGRIS, also uses a sampling-based framework but continuously optimizes and refines plans online as the robot acquires new information. This adaptive refinement is crucial for long-horizon planning scenarios where optimal paths are difficult to determine in a single planning cycle. Through improvements in tree-building logic and novel belief space node embeddings, IA-TIGRIS achieves sufficient computational efficiency for on-board deployment. We validate our method through extensive simulation testing and demonstrate efficient online planning capabilities on hardware across two distinct UAV systems.

III. PROBLEM FORMULATION

This work addresses the challenge of maximizing data gathered by a robot within the specified budget constraints of the system, a problem formally known as the IPP problem. Our problem formulation is defined as

$$\mathcal{T}^* = \arg \max_{\mathcal{T} \in \mathbb{T}} I(\mathcal{T}) \text{ s.t. } C(\mathcal{T}) \leq B.$$

We let \mathcal{T} represent the sensor trajectory within the set of feasible trajectories \mathbb{T} , and $C(\mathcal{T})$ be the cost function for a given trajectory. An example of potential costs would be trajectory length, energy usage, or time and would not exceed the budget constraint B . Lastly, $I(\mathcal{T})$ is the reward or information gain from a trajectory, and an optimal trajectory \mathcal{T}^* is found that maximizes the information gain and does not exceed the budget B .

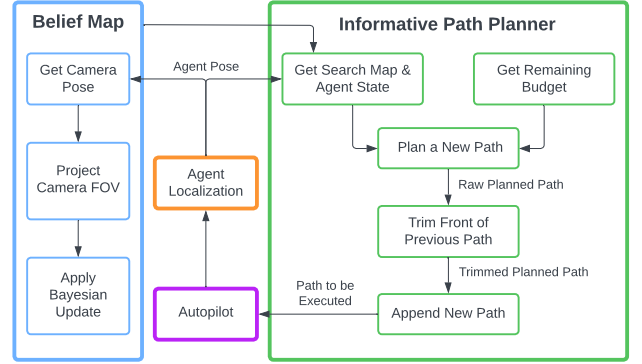


Fig. 2. Overview of the IA-TIGRIS planning framework. As the robot is executing the current path, the belief map is updated using the current robot position. Whenever a new plan is initiated, the current robot position, belief map, and remaining budget are passed to the planner. The new path is merged into the previous path and given to the autopilot for execution.

IV. PROPOSED APPROACH

This section details our proposed approach for informative path planning online using incremental and adaptive methods. A high level overview of our framework is shown in Fig. 2. Subsection IV-A provides a thorough explanation of the core algorithm, including the main planning loop and the graph update procedure, elucidating the steps involved in sampling, steering, and constructing the tree of potential paths. Subsection IV-B discusses the strategy to enable adaptive replanning with the presented algorithm. Finally, Subsection IV-C explores the techniques used to incrementally update the path, enhancing the efficiency and responsiveness of the planning process. Subsections IV-D and IV-E explain how the belief space and observation model integrate into the planner, and Subsection IV-F presents our reward models.

A. Algorithm Overview

The IA-TIGRIS algorithm comprises two main components: the main planning loop (Algorithm 1) and the graph update procedure (Algorithm 2). Let the notation $X \stackrel{\pm}{\leftarrow} \{\mathbf{x}\}$ and $X \stackrel{\leftarrow}{\leftarrow} \{\mathbf{x}\}$ represent the operations $X \leftarrow X \cup \{\mathbf{x}\}$ and $X \leftarrow X \setminus \{\mathbf{x}\}$ respectively. The IA-TIGRIS planning loop takes as input the agent start pose, x_{start} , the state space \mathcal{X} , the remaining budget B , the remaining allowed planning time T , the extend distance for tree building Δ , and the radius for neighbor selection R .

At the beginning of planning, the set of vertices V is empty. The initial information I_s at the start pose x_{start} is calculated by $I(\cdot)$, and the initial cost C is set to 0. The tuple n_{start} is initialized and added to the set of vertices V , while the set of edges E and the closed set of vertices V_{closed} are initialized as empty. The graph G is initialized as $G \leftarrow (V, E)$.

The Algorithm 1 then loops until the computation time exceeds the allowed planning time T . During each iteration of the loop, a sample x_{sample} is drawn from the state space \mathcal{X} using the INFORMEDSAMPLE function which is a weighted sampler based on the reward for viewing a state in the

Algorithm 1: IA-TIGRIS

Input : \mathbf{x}_{start} : Agent start pose
 \mathcal{X} : State space
 B : Budget
 T : Allowed planning time
 Δ : Extend distance for tree building
 R : Radius for neighbor selection

Output: \mathcal{T} : Planned path

```

1 if  $V = \emptyset$  then
2    $I_s \leftarrow I(\mathbf{x}_{start}); C \leftarrow 0$ 
3    $n_{start} \leftarrow \{\mathbf{x}_{start}, I_s, C\}$ 
4    $V \leftarrow n_{start}; E \leftarrow \emptyset; V_{closed} \leftarrow \emptyset; G \leftarrow (V, E)$ 
5 end
6 else
7    $\text{UPDATEGRAPH}(\mathbf{x}_{start}, B)$ 
8 end
9 while computation time  $< T$  do
10   $\mathbf{x}_{sample} \leftarrow \text{INFORMEDSAMPLE}(\mathcal{X})$ 
11   $n_{nearest} \leftarrow \text{NEAREST}(\mathbf{x}_{sample})$ 
12   $\mathbf{x}_{feas}, e_{feas} \leftarrow \text{STEER}(n_{nearest}, \mathbf{x}_{sample}, \Delta, X_{free})$ 
13   $\text{ADDPPOSETOGRAPH}(\mathbf{x}_{feas}, e_{feas}, n_{nearest}, \Delta, R, B)$ 
14   $N_{near} \leftarrow \text{NEAR}(\mathbf{x}_{feas}, R, V \setminus V_{closed})$ 
15  for  $n_{near} \in N_{near}$  do
16    if  $n_{near} \neq x_{feas}$  and  $n_{near} \neq n_{nearest}$  then
17       $\mathbf{x}_{new}, e_{new} \leftarrow \text{STEER}(n_{near}, \mathbf{x}_{feas}, \Delta, X_{free})$ 
18      if  $\mathbf{x}_{new} \neq n_{near}$  then
19         $\text{ADDPPOSETOGRAPH}(\mathbf{x}_{new}, e_{new}, n_{near}, \Delta, R, B)$ 
20      end
21    end
22  end
23 end
24 return  $\mathcal{T} \leftarrow \text{BESTPATH}(G)$ 

```

belief space. This is done by first conducting the weighted sample in the belief space and then uniformly sampling in the subset of the configuration space that views the sampled belief space state while respecting desired observation constraints. Informed sampling focuses paths on areas of higher reward rather than uniformly sampling in the search space.

The nearest node $n_{nearest}$ in the graph G to x_{sample} is identified, and the algorithm attempts to steer from $n_{nearest}$ to x_{sample} within a specified distance Δ while checking for collisions, resulting in a feasible pose x_{feas} and an edge e_{feas} . In contrast with [30], the new pose and edge are immediately evaluated to be added to the graph G using the ADDPPOSETOGRAPH function, allowing the neighbor selection radius R to be less than the extend distance Δ .

The algorithm then searches for nearby nodes N_{near} within a radius R of x_{feas} that are not in the closed set V_{closed} . For each neighbor n_{near} in N_{near} , if n_{near} is distinct from x_{feas} and $n_{nearest}$, the algorithm attempts to steer from n_{near} to x_{feas} . If the new pose x_{new} is distinct from n_{near} , the pose and edge evaluated to be added to the graph G using the ADDPPOSETOGRAPH function. This neighborhood expansion structure is different than [30] in that it now allows for neighboring nodes to extend toward x_{feas} even if it did not add and edge connecting to $n_{nearest}$.

After the computation time is exhausted, the algorithm extracts the best path \mathcal{T} from the graph G using the BESTPATH function. This function simply returns the path with the highest information reward in the graph.

Algorithm 2: ADDPOSETOGRAPH

Input : \mathbf{x}_{new} : New pose
 e_{new} : Edge from n_{parent} to \mathbf{x}_{new}
 n_{parent} : Parent node in graph
 Δ : Extend distance for tree building
 R : Radius for neighbor selection
 B : Budget

```

1  $I_{new} \leftarrow I(\mathbf{x}_{new}, e_{new}, n_{parent})$ 
2  $C_{new} \leftarrow C_{n_{parent}} + \text{Cost}(e_{new})$ 
3  $n_{new} \leftarrow \{\mathbf{x}_{new}, I_{new}, C_{new}\}$ 
4 if not  $\text{PRUNE}(n_{new})$  then
5    $E \leftarrow E \cup \{e_{new}\}$ 
6    $V \leftarrow V \cup \{n_{new}\}$ 
7    $G \leftarrow (V, E)$ 
8   if  $C_{new} = B$  then
9      $V_{closed} \leftarrow V_{closed} \cup \{n_{new}\}$ 
10  end
11 end

```

The ADDPPOSETOGRAPH function, outlined in Algorithm 2, handles the addition of a new pose x_{new} and edge e_{new} to the graph G . The information I_{new} for the new pose is calculated, and the cumulative cost C_{new} is computed by adding the cost of the edge e_{new} to the cost of n_{parent} . A new node n_{new} is created as a tuple containing the new pose, information, and cumulative cost. The node n_{new} is then checking by the PRUNE function. The pruning function checks nearby nodes within a radius to see if they contain a better solution. Because most of the nodes in the tree are not full paths, the upper bound on their rewards are compared. For more aggressive pruning, heuristics can be used for this comparison. In our case we use the heuristic of checking if a nearby node has a lower cost and higher current reward, but this heuristic can have implications on finding the optimal solution. If n_{new} passes the pruning check, the edge e_{new} and node n_{new} are added to the sets E and V , respectively, and graph G is updated. If the cumulative cost C_{new} equals the budget B , the new node n_{new} is added to the closed set V_{closed} .

B. Adaptive Replanning

For environments where the world is static and measurements are deterministic, global plans could be static and created once before flight. Having a single, static plan would also work well in situations when onboard computation is restricted, there is high confidence the global path is optimal, the executed path will be perfectly followed, and the predicted information gain will be close to the actual information gain. However, there are many cases where the plan would need to be adjusted due to disturbances and modified due to new information. When disturbances cause deviations from an expected observation, the path can be replanned during path execution to re-observe locations and adjust the path according to the current information map.

The adaptability of IA-TIGRIS is due to its ability to continuously replan the global trajectory online. The updated paths take into account the current world belief updated by all observations. This brings robustness, as executed paths may

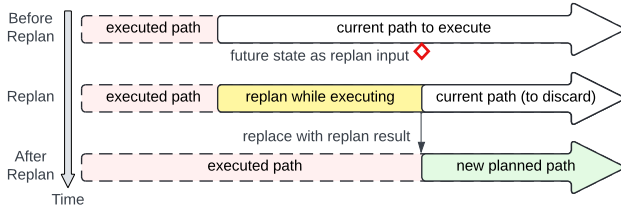


Fig. 3. Visualization of the online replanning procedure. The future robot state is used as the starting point for the next plan. The newly-planned path is merged with the previous path.

not follow the planned path due to disturbances and lead to differences in the planned versus expected observations.

The Algorithm 1 described above is a planning procedure that generates a path from the starting configuration. To replan adaptively during flight, a starting configuration is chosen that is time T in the future along the previously-planned path. Similarly, the budget B is updated based on remaining flight time based on the current battery levels or mission constraints. The new path is merged with the previous path, keeping any portion of the previous path before the starting pose of the new path. This process is visualized in Fig. 3.

C. Incremental Planning

When replanning online, discarding the previous planning graph wastes valuable information and forces the planner to start from scratch. By using an incremental approach, the planner can reuse the previous planning efforts, improving efficiency and enabling the next global plan to refine the earlier one. This often results in higher-quality paths. Even when the budget and belief map remain unchanged between replans, many scenarios—such as large budgets or small areas relative to the budget—can benefit from incremental refinement. In challenging planning situations, this approach allows the planner to iteratively expand the search tree, continuing to explore and evaluate potential paths.

To enable incremental planning, our method recycles as much of the previously-built graph as possible, rather than create a new graph whenever a plan is requested. Even when the belief map and budget have changed, recycling the previous graph offers significant benefits. The previous graph has already been validated for collisions and adheres to the vehicle’s motion model, allowing the planner to build upon prior work and save computational resources while maintaining accuracy.

To reuse the previous tree, Algorithm 1 first checks if the vertex set V is empty. If it is not empty, then rather than initializing the graph, it calls the function `UPDATEGRAPH`. This function first finds where the starting point for the next plan lies within the previous plan. When a matching node is found in the previous plan, all nodes and edges before that node are pruned away. The remaining portions of the graph are checked for the budget constraint and the information gain up to each node are updated based on the current information map. This is done by efficiently traversing the tree recursively from the starting node working down to all leaf nodes. The

planner then uses the updated graph to plan as normal. A high-level overview of this process is shown in Fig. 4.

D. Belief Space Representation and Node Embedding

In informative path planning, the information within a space can be represented using various models, such as Gaussian mixture models, Gaussian process regressions, grids, or voxels. This belief space can encode different types of information. For example, it might represent the probability of an object of interest being located in specific regions of the space. The choice of belief space formulation is important, as it directly influences the planning process by guiding search efforts and behaviors. An effective representation for a specific system, application, and planner balances computational complexity, memory requirements, and the ability to perform operations on the belief model.

In this work, we adopt a grid-based representation of the belief space. Specifically, the search space is discretized into a grid of cells, where each cell i is associated with a binary random variable X_i indicating the presence ($X_i = 1$) or absence ($X_i = 0$) of an object of interest. The probability $P(X_i)$ represents our belief about an object being located in cell i . This grid-based representation is computationally straightforward to update with new or predicted observations using a Bayesian framework and an appropriate sensor model.

1) *Belief Space Node Embedding*: The nodes in the planning tree maintained by the IA-TIGRIS algorithm store the necessary information to represent the evolving belief space. The information gain up to a given node is computed based on the change in entropy within the grid cells observed by the agent’s sensor footprint during traversal from the root node to the current node.

A straight-forward approach to calculating the information gain for a given node consists of traversing the tree from the root all the way to the given node. It is necessary to evaluate the entire trajectory because the information gain can be not modular and previous observations affect the information gain of future observations. Calculating the additional information gain contributed by a new node and edge requires knowledge of the belief state of the search map at the previous node. However, this approach of calculating information gain starting at the root node is computationally inefficient and slow. Let n be the number of cells in the search map, m be the number of nodes in the tree, k be the number of nodes in a trajectory, and j be the upper bound of cells updated by a node in the tree. The temporal complexity of this method is $\mathcal{O}(kj)$ and the memory complexity is $\mathcal{O}(n)$.

One approach to speeding up computation is to store the entire search map within each node. In this approach, the information gain for a new node is simply the sum of the parent node’s information gain and the contribution of the new node. This method results in a temporal complexity of $\mathcal{O}(j)$ for calculating the information gain of a new node and a memory complexity of $\mathcal{O}(nm)$. While feasible for small maps, this method becomes impractical for large-scale maps relevant to the domains and applications considered in this work due to its high memory requirements.

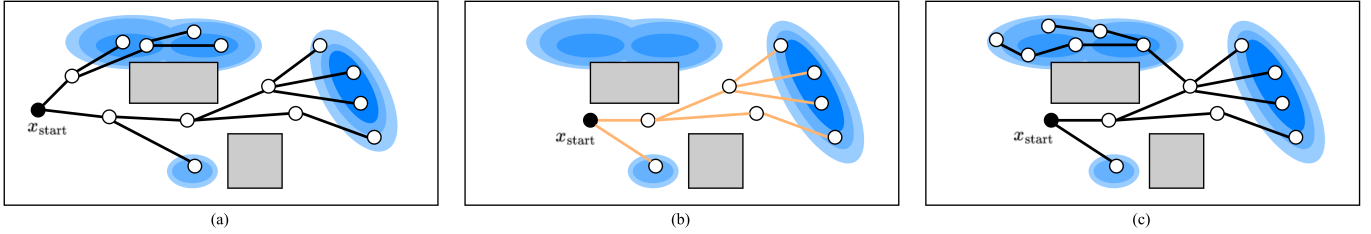


Fig. 4. An illustration of the incremental planning and refinement process in IA-TIGRIS. (a) The global planner first generates long-horizon paths to maximize predicted information gain. (b) At the start of each new planning cycle, infeasible portions of the tree, based on the executed trajectory and the current plan, are pruned. The remaining tree is then updated by recomputing information gain and cost based on the latest belief state and available budget, which is significantly more efficient than rebuilding the tree from scratch. (c) The tree is further expanded and refined for the duration of the planning cycle, after which the process repeats.

To efficiently compute the information gain for a new node, we introduce a node embedding strategy that eliminates the need for a full traversal of the planning tree from the root to the current node. Instead of storing the complete belief state in each node, we use a sparse representation that records only belief updates. A hash map efficiently tracks modifications to belief probabilities, reducing memory complexity while preserving the ability to compute information gain incrementally. This allows for efficient calculations of the information gain for a new node while maintaining computational efficiency without sacrificing accuracy.

The temporal complexity of calculating the information gain for a new node is now $\mathcal{O}(j)$, and the overall memory complexity of this belief space representation is only $\mathcal{O}(jm + n)$. As long as $j \ll n$, this approach is much more memory-efficient than the naive approach of storing the complete belief state in each node. Each node in our tree now contains the cumulative information gain along the path, current state of the agent, path cost, and edge path.

While implementing this embedded method, we observed the significant impact on computation time from selecting efficient keys for the hashmap. Using strings as keys resulted in substantial overhead due to frequent string-to-integer conversions. Even transitioning from a two-integer key to a single-integer key yielded a notable improvement in performance and is the approach we use in our implementation through a simple index-to-key conversion. Given that cell value lookup operation occurs frequently, optimizing its efficiency was highly impactful for accelerating the expansion rate of the search tree.

By incorporating this belief space node embedding strategy, our planning framework efficiently maintains an accurate representation of the evolving belief space within the search tree. This enables the planner to greatly reduce computational overhead and create higher quality paths.

E. Sensor Modeling

The updates to our belief map are dependent on the sensor model, which captures the performance characteristics of the perception system employed. There are many environmental factors that affect the performance of a sensor, such as visibility and range, which can be incorporated into this model.

For our approach, we formulate the sensor model as a piecewise function and is implemented as a lookup table. For

a given range r and binary measurement Z , this table maps the range of the object from the sensor to the corresponding true positive rate (TPR) $P(Z|X, r)$ and true negative rate (TNR) $P(\bar{Z}|\bar{X}, r)$ of an object detection model. A typical range-based detection model will have better performance at close ranges and then tapers off as the distance increases.

By maintaining a lookup table of these sensor models, we can easily incorporate different sensor modalities and their corresponding capabilities into the planning framework. The sensor model can be derived from actual test data and easily integrated into the framework rather than having to fit a function to the results.

The sensor model for belief map updates is a crucial component of the overall planning framework, as it directly affects the information gain computed for each node in the IA-TIGRIS tree. Accurately modeling the sensor’s performance characteristics enables the planner to make informed decisions, resulting in more effective exploration and search strategies that align with actual sensor capabilities. Conversely, inaccuracies in the sensor model can lead to overconfidence in observed areas or unnecessary revisits to regions that have already been sufficiently searched.

F. Information Reward Models

The information reward function $I(\cdot)$ used in our framework is not constrained to being modular and could be time-varying or even submodular, depending on the specific requirements of the application. In this work, we have implemented an objective of reducing the overall entropy of the belief space. As defined in Section IV-D, our belief space represents the probability of the presence of an object of interest in a cell. The reward for one cell $I(X_i)$ is calculated by finding the difference between the initial entropy and the final entropy after updating the belief with the measurements and sensor model defined in Section IV-E.

The Shannon entropy of a cell is calculated by

$$H(X_i) = -P(X_i) \log P(X_i) - P(\bar{X}_i) \log P(\bar{X}_i) \quad (1)$$

where X_i represents the event that the cell is occupied and \bar{X}_i denotes its complement, the event that the cell is free.

The entropy reduction due to a single positive measurement would be calculated as

$$\Delta H(X_i|Z) = H(X_i) - H(X_i|Z)$$

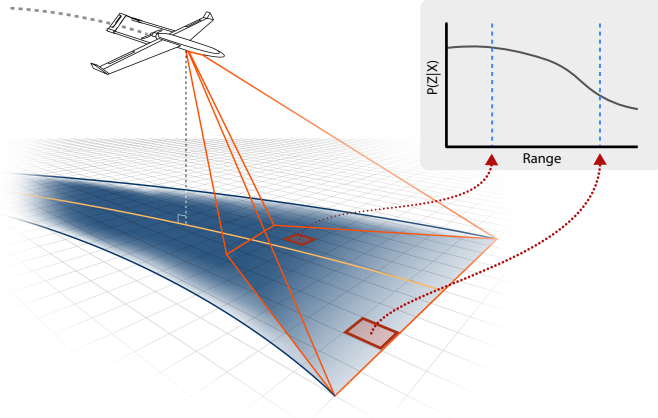


Fig. 5. An example of how the grid cells rewards are estimated given a planned trajectory. The cells that are closer to the center of the trajectory have a smaller minimum distance than cells farther from the center of the trajectory, leading to a larger change in entropy for the closer cells.

where $H(X_i)$ is given by (1), and $H(X_i|Z)$ is the entropy conditioned on the sensor measurement Z .

The final information gain for a trajectory $I(\mathcal{T})$ would be

$$I(\mathcal{T}) = \sum_i^I H(X_{i,init}) - H(X_{i,final})$$

where $X_{i,init}$ is the initial belief state of cell i , and $X_{i,final}$ is the final belief state.

1) *Information Reward Estimation:* When adding a new node in the planning tree, the approach for estimating the information gain may vary depending on the modularity and temporal dependence of the information function. In the case of a modular and temporally independent function, the reward for a new node can be simply appended to the cumulative reward along the path. Alternatively, if the information function exhibits non-modularity or temporal dependence, the entire trajectory up to the current node may need to be re-evaluated to determine the appropriate reward. Because we do not yet know the future measurements for each cell, the information gain for the planned path must be estimated.

One option would be to compute the expectation of the information gain given all possible future measurements. However, this can be computationally expensive and infeasible. We avoid this by following the approach of [30], [36] and use an optimistic approximation of the expected reward. Specifically, we assume a positive measurement Z if $P(X) \geq 0.5$, and a negative measurement otherwise. This leads to the following cell reward function for a single measurement:

$$I(X_i) = \begin{cases} \Delta H(X_i|Z) & P(X_i) \geq 0.5 \\ \Delta H(X_i|\bar{Z}) & P(X_i) < 0.5 \end{cases} \quad (2)$$

To compute the information reward along a path, the sensor footprint is projected onto the surface plane to determine all the cells it contains. The reward for each cell is calculated using (2) and then aggregated. This process becomes more intricate when incorporating graph edges into the reward computation. Discretizing the trajectory between nodes into individual views creates imperfect overlaps due to the non-square sensor footprint, potentially omitting some grid cells

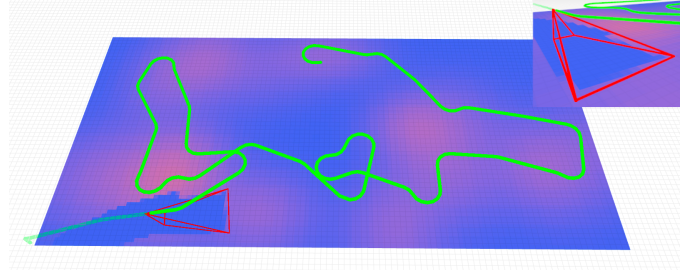


Fig. 6. Example results for IA-TIGRIS after a replanning step in our simulation environment. Pink regions represent regions of high entropy while blue regions are areas of low entropy. The red projection shows the camera frustum while the green line represents the planned path.

from the edge reward calculation. Mitigating this issue requires significant overlap between sensor footprints, which, in turn, greatly increases the computation time for updating grid cell beliefs. Rather than selecting a discretization resolution for the trajectory, we compute a conservative approximation of the edge reward by updating all cells within the view of edge trajectory, using the closest viewing distance along the path for each cell. This approach ensures that all cells along the edge are accounted for, with each belief value updated using a measurement taken when the sensor is closest to that cell. A visualization of this reward estimation is shown in Fig. 5.

2) *Priority-dependent Rewards:* In the case where certain areas of an environment or spatial information are more important than others, we introduced the ability to weight the information reward by a priority scalar, p_i , representing the priority of cell i . This approach provides finer control over the UAV behavior by allowing the entropy of different cells to be weighted unequally. Assigning a higher priority to one prior over another results in paths that favor observations of the higher-weighted prior. For example, this is useful when one type of object is more important than another, and the prior spatial distributions are concentrated in distinct areas of the search space (as demonstrated in Section V-C3).

3) *Time-dependent Rewards:* The IPP formulation maximizes total information gain over the entire mission without explicitly relating the reward to the timing of observations—rewards are time-independent. However, in some applications, operators may prefer prioritizing areas of high information gain earlier in the trajectory rather than later.

We introduce the ability to create time-dependent reward that decreases the reward value for all cells over the mission duration, resulting in plans that prioritize visits to areas of high information gain early in the plan. This works especially well when paired with priority-dependent rewards, as introduced in Section IV-F2. The UAV will be biased toward visiting the higher priority priors early in the plan, and the operator can even roughly dictate the order to visit areas through differing priority weights and using the time-dependent reward decay function.

In our use cases, we implement a simple reward decay function

$$\Gamma(t) = \begin{cases} \gamma & t \geq \gamma_t \\ \beta t + 1 & t < \gamma_t \end{cases}$$

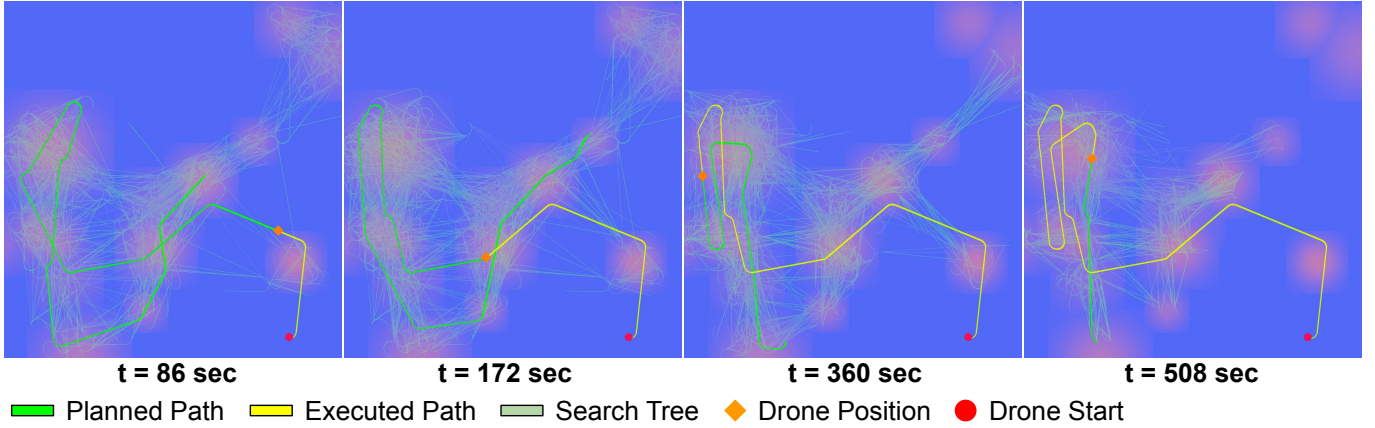


Fig. 7. IA-TIGRIS continuously replanning and refining the global path over the duration of the simulation. These snapshots show how the path is refined online to maximize information gain. The search tree is also visualized and shows how the plans focus on the areas of high information gain and take into account the remaining budget.

where $\Gamma(t) \in [\gamma, 1]$ and γ is the floor value of the decay function. β is the decay rate and $\gamma_t = (\gamma - 1)/\beta$ is the time where the function output becomes the floor value γ . This gives a linear decay until the floor value.

Combining our decay function $\Gamma(t)$ and cell priority values p_i creates a priority and time dependent reward function

$$I(X_i, t) = \begin{cases} p_i \Gamma(t) \Delta H(X_i | Z_i) & P(X_i) \geq 0.5 \\ p_i \Gamma(t) \Delta H(X_i | \bar{Z}_i) & P(X_i) < 0.5 \end{cases}$$

V. SIMULATION EVALUATION & RESULTS

To rigorously evaluate the performance and benefits of IA-TIGRIS, we first conduct tests in a simulation environment. These experiments include ablations to assess the impact of key design decisions, as well as Monte Carlo evaluations comparing IA-TIGRIS against baseline methods.

A. Simulation Framework

We use a simplified simulator, shown in Fig. 6, to enable rapid development and validation of our approach. The simulation employs a constant-velocity motion model for the fixed-wing UAV. To account for the effects of banking on observations, we compute the orientation change between consecutive waypoints. If this change exceeds a threshold, the UAV is considered to be banking, and the belief space is not updated during this period. This reflects the fact that the camera is primarily pointed toward the sky during banking and is also affected by increased motion blur.

When the UAV reaches a commanded waypoint within a specified Euclidean distance threshold, the next waypoint in the list becomes the new commanded waypoint. During replanning, a newly generated path is merged with the existing path, incorporating the updated trajectory starting from the beginning of the new path. A simple proportional (P) controller is used to regulate heading and altitude, guiding the UAV between waypoints.

The UAV commanded speed is 25 m/s, with a planning time of 10 seconds and a the flight altitude of 50 m. The turning radius is 100 m, and the onboard camera is pitched 30

degrees from horizontal with a 36.9-degree field of view. The belief space grid cells are 30 m, and the total budget for flight distance is 15,000 m. To accelerate testing, the simulation runs at twice the real-time speed, with results subsequently rescaled to match real-time conditions.

Fig. 7 presents four snapshots from a simulation. The planned path is shown in green, the executed path in yellow, the robot's current position as an orange diamond, and the starting position as a red circle. Early in the simulation, the planned trajectory makes two passes over the larger clusters of high-entropy regions, which represent areas of high uncertainty. The search tree explores a wide range of paths across these regions to maximize information gain, refining its evaluation over time. As the planning cycle progresses, the search tree is iteratively updated through tree recycling, which improves computational efficiency by retaining and modifying previous solutions rather than replanning from scratch. At $t = 180$, the plan adapts by doubling back to the middle-left region, due to finding a more rewarding path. Toward the end of the simulation, the effect of the budget constraint becomes apparent, as the search tree no longer extends into the upper-right corner of the search area.

B. Metrics

The primary metric for evaluating the success of our plan is the information gain along the executed path, quantified as the change in total entropy of the belief space from the initial to the final state. To facilitate interpretation and comparison across tests, we report this as the percent reduction in entropy. Initially, the entropy reduction is zero, as no observations have been made. As the robot gathers information, the entropy decreases, reflecting an improved understanding of the environment. This reduction continues to accumulate throughout the simulation as new observations refine the information map.

C. IA-TIGRIS Ablations

We conduct ablation experiments to evaluate the impact of incremental and adaptive planning, belief space node em-

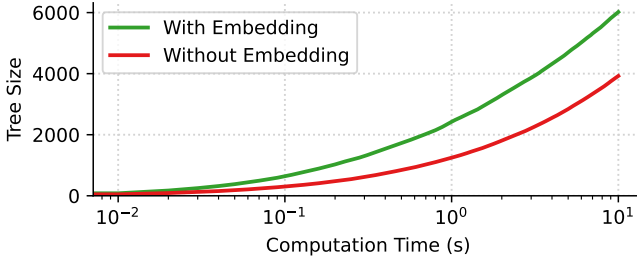


Fig. 8. Tree size vs computation time for 100 trials.

beddings, priority and time dependent rewards, and planner parameters.

1) *Incremental and Adaptive Planning Evaluation:* We first evaluate the efficiency of recycling a search tree compared to building a new one for each planning cycle. For IA-TIGRIS to be both adaptive and incremental, reusing and recycling previous planning efforts must be computationally efficient. As explained in Section IV-C, each planning begins by pruning irrelevant trajectories, checking budget constraints for remaining nodes, and updating information gain based on the current belief map. If these updates consume too much planning time, there will be insufficient time left to refine and extend the trajectory.

Our implementation of IA-TIGRIS demonstrates that recycling a previously built tree is significantly more efficient than constructing a new tree from scratch. For example, a tree that takes 10 seconds to build requires less than 0.2 seconds to update under our planner settings and test environment. This efficiency gain allows the entire tree to be recycled and extended with the remaining planning time, even if none of the previous plan was executed. By avoiding the computational overhead of trajectory generation, neighborhood search, and collision checking, tree recycling results in faster updates and enables the planner to generate improved paths within the same time constraints.

To quantify the impact of tree recycling and replanning, we conducted 50 tests in the simulation framework described in Section V-A. Without replanning, the average reduction in entropy was 20.4%. Introducing replanning without tree recycling improved this to 23.1%, a 13.2% increase in performance. Even in the absence of environmental disturbances, replanning improves path quality by addressing mismatches between estimated and actual information gain, particularly as the planning horizon shortens due to decreasing budget. Incorporating incremental planning with tree recycling further increased the reduction in entropy to 25.4%, a 24.5% improvement compared to replanning without tree recycling. This highlights IA-TIGRIS’s to refine and improve the previous global plan.

As expected, the benefits of replanning and refinement become more pronounced when planning time is reduced. When the allowed planning time is reduced to 3 seconds, the performance difference between no replanning and replanning with tree recycling increases to 25.8%. This gap would widen further for even shorter planning times, where initial plans tend to be of lower quality. However, as planning time decreases, a

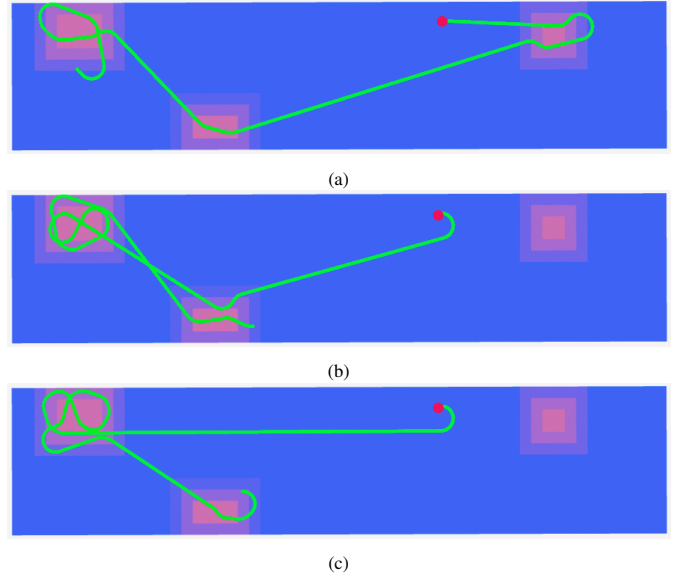


Fig. 9. Examples showing how modifying the priority and time-based rewards effects behavior. The starting point is shown in red and the planned path in green. (a) The base case with equal priorities. (b) A higher priority on the far left prior causes the drone to spend more of its budget observing that space. (c) With time-based rewards, the drone visits the high priority prior as quickly as possible to maximize reward.

larger portion of the time is allocated to recycling previous plans rather than expanding the tree, leaving less time for refinement. This introduces a tradeoff between path quality and responsiveness; more frequent replanning improves adaptability to new information, while longer planning cycles allow for more extensive trajectory refinement.

2) *Belief Space Node Embedding Analysis:* We evaluated the impact of belief space embedding on the efficiency of our planning. Calculating the information gain for a trajectory can take up a disproportionate amount of the planning time if not implemented well. We found that in our typical testing environments, using our belief space embedding in the tree nodes reduced the time to compute the information gain by around 80-95%. This increase in speed only resulted in an additional ~ 20 MB of memory usage for the search tree.

Fig. 8 shows the tree size of the first plan vs time for 100 trials on random simulation environments. Due to the reduction in time to add each new node to the planning tree, the tree size is much larger at any point during planning.

Our embedding also has a profound impact on the speed of recycling the search tree between plans. Previously the information gain at each node would be calculated individually when recycling the tree, with the nodes toward the base of the tree getting evaluated many times. Now, the tree can be updated recursively from the root to the leaves without evaluating the information at any node more than once. When tested in our typical environments, this cut down the time to rebuild a tree from ~ 180.93 μ s per node to ~ 15.48 μ s per node.

We also evaluate the impact of belief space embedding by using Google Benchmark [42] on an extremely large environment. For these benchmark tests, the number of nodes in the trajectory was $k = 7$, the number of grid cells in the

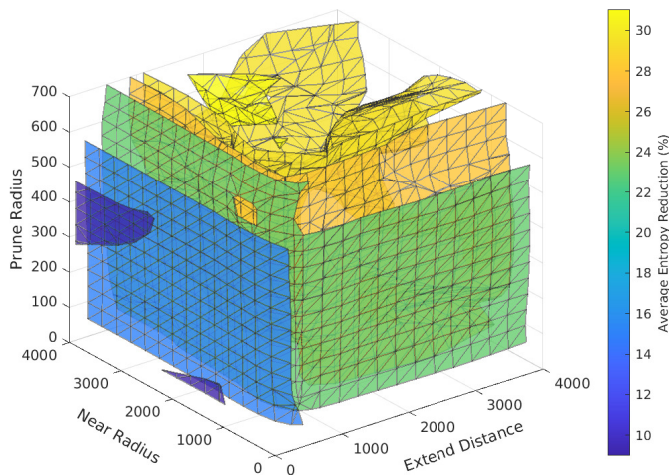


Fig. 10. An isosurface plot showing the results of the global parameter search. Each surface shows given parameters that result in similar average percent of entropy reduction over a set of tests.

search space was $n = 39,841,344$, and the number of grid cells updated by the new node was $j = 11,984$. The time to evaluate the information gain for a new node decreased from 43 ms to 1.9 ms, a 96% improvement. This led to the size of the search trees to on average be more than double in size.

3) *Priority and Time Dependent Rewards Evaluation:* To illustrate the impact of priority-dependent and time-dependent rewards, we conduct a simulation with the results shown in Fig. 9. To make the effect of flight paths more clear, the camera is pitched down so that the flight path coincides more closely with what is observed by the sensor. The example scenario has three clusters of uncertainty in the search space.

Fig. 9a shows the base case where three areas of uncertainty have equal priority. The planned path visits the closest cluster first and then travels to the left side, viewing all three clusters. Fig. 9b demonstrates when the cluster on the far left is adjusted to have a higher priority. The path no longer visits the cluster on the right in favor of saving the budget to expend more effort in searching the higher-priority region. When adding a time-based reward along with the priority, Fig. 9c shows how the path first visits the high-priority prior before moving on to the other prior on the left. The time-based reward causes the order of observations to affect the total reward.

4) *Planner Global Parameter Search:* We investigate the effects of the extend distance Δ , the near radius R used in $\text{NEAR}(\cdot)$, and the pruning radius used in $\text{PRUNE}(\cdot)$ within IA-TIGRIS, as outlined in Section IV-A. To do this, we perform a global parameter search across 25 randomly generated environments. Each environment was $5 \text{ km} \times 5 \text{ km}$, with a prior belief map consisting of a random number of Gaussian distributions with varying locations, means, and standard deviations. The planning loop was given a 10-second planning time, and the agent continued to observe the space until budget was expended.

Using percent reduction in entropy as the performance metric, we visualize the results in an isosurface plot, shown in Fig. 10, where higher percentages indicate greater information gain. The results suggest that, for the sampled environments,

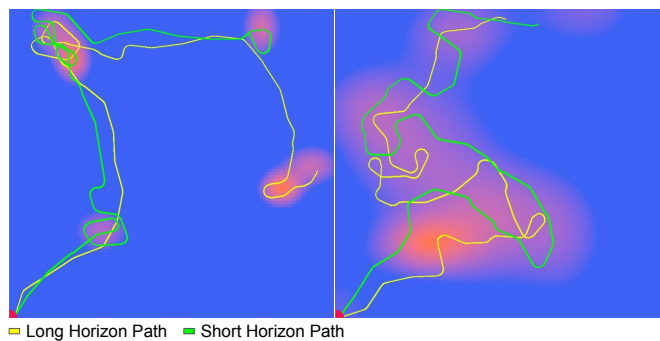


Fig. 11. A comparison of IA-TIGRIS when planning over a long horizon versus a short horizon. Long-horizon planning enables IA-TIGRIS to allocate the entirety of its budget efficiently and is able to view all of the high-entropy clusters in the example on the left. In the example on the right, short-horizon planning leads to less smooth paths with slightly higher information gain, as the high-entropy areas are connected and have lower entropy the farther they are from the starting position.

planner performance improves as the extend distance and near radius are larger. If one is much smaller than the other, performance greatly reduced. However, the relationship between pruning radius and performance is less clear, though a slight performance increase is observed as the pruning radius grows.

The pruning radius primarily affects the planned path length at the start of a test. A very small pruning radius results in paths shorter than the 15 km budget, likely because a denser tree limits tree depth. Similarly, reducing the extend distance below 500 m leads to shorter initial plans, suggesting that both parameters play a role in determining tree expansion.

We find that as the extend distance increases, maintaining a sufficiently large near radius is crucial for sustaining performance. If the near radius drops below the extend distance, performance declines. Meanwhile, the pruning radius can be set relatively high without significant performance loss, and doing so allows for longer planned paths. Additionally, the CPU performance of a given system may influence the optimal parameter settings, suggesting the need for adjusting parameters based on computational resources.

The parameter with the highest performance in our testing had the combination of an extend distance and near radius that balanced expansion while still creating a dense tree, and a large pruning radius to act as a stronger heuristic for high-quality paths. For our subsequent simulation testing, we selected an extend distance of 1500 m, near radius of 1500 m, and a pruning radius of 600 m.

5) *Long-Horizon Planning:* To demonstrate the effects of long and short horizon planning, we ran a simulation on two different maps with varying information distributions as seen in Fig. 11, where the pink region have high entropy and blue regions have low entropy. The environment on the left side of the figure shows a distribution with clusters of information scattered across the space while the environment on the right shows a denser distribution where the various areas of high entropy overlap. For short-horizon planning, IA-TIGRIS considers a planning horizon of up to 5000 m, rather than planning over the entirety of the remaining budget. The long-horizon planning starts with the entire budget of 15000 m and uses the entire remaining budget for every new plan in

the planning process.

For the clustered information map on the left, the long horizon path search over more clusters and achieves a higher overall information gain compared to the short horizon path. This is because the short-horizon planner takes myopic actions, consuming the majority of its budget on the first two clusters. By the time it reaches the third cluster, it exhausts its budget and is unable to reach the last cluster. In contrast, the long horizon planner strategically balances its budget across all four clusters, enabling higher information gain.

For the dense information map on the right, the long-horizon planner generates a smoother path and extends farther into the space compared to the short-horizon planner. However, the long horizon planner allocates a smaller portion of its budget on the highest information gain area near the start position. As a result, the short-horizon planner achieves a slightly better total information gain by prioritizing immediate rewards and concentrating its budget on the highest information cluster close to the starting position.

From these two maps, we observe that the long-horizon planner excels in environments with clustered information where reasoning over long horizons is essential to avoid myopic choices and balance the allocation of budget. The short-horizon planner does perform well in environments with densely distributed information, where following local gradients of information gain can lead to effective solutions. These findings suggest that the impact of the planning horizon on system performance can be environment-dependent. In our testing framework and applications, planning over the entire budget typically yields the best results, as our prior information maps often feature clustered regions of high information gain.

D. Baseline Planners

To evaluate the performance of IA-TIGRIS, we compare it against several baseline methods. In the following section, we describe these baselines, their implementation details, and their respective advantages and limitations, particularly in the context of information gathering in large, high-dimensional search spaces. The simulation framework and vehicle parameters remain consistent across all planners, and each method is allowed to replan during testing.

1) *Monte-Carlo Tree Search*: Monte Carlo Tree Search (MCTS) can be a powerful technique for finding feasible and optimal paths in complex environments. It is a heuristic search algorithm that builds a search tree incrementally through repeated simulations. At each iteration, it selects a node to explore based on a selection policy (often the Upper Confidence Bound or UCB1 algorithm), expands the tree by adding possible actions from that node, runs a simulation from the newly added node, and updates the statistics of nodes along the path traversed during the simulation.

The UCB1 (Upper Confidence Bound) algorithm is a technique commonly used in the context of multi-armed bandit problems and Monte Carlo Tree Search (MCTS) for balancing exploration and exploitation. It helps in selecting actions or nodes that are likely to yield high rewards while also exploring less-frequented options to gather more information about their potential rewards.

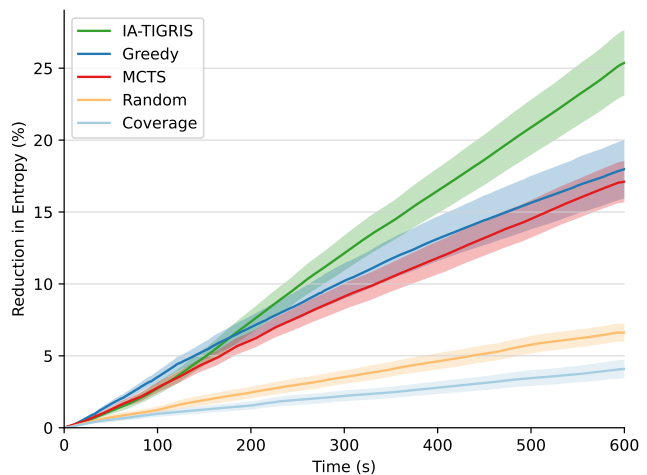


Fig. 12. The Monte Carlo simulation results for the planners. The plots show the average percent reduction in entropy over the course of the simulations, and the shading shows the 95% confidence intervals. IA-TIGRIS outperforms all of the baselines.

We formulate our UCB score in the following manner,

$$UCB_{\text{node}} = \frac{I(X_{\text{node}})}{\alpha} + C \times \sqrt{\frac{\ln(N_{\text{tree}})}{N_{\text{node}}}}$$

Here $I(X_{\text{node}})$ denotes the estimated information gain from the node, α denotes the normalization factor which is given by $\frac{B}{v_{\text{desired}}}$, B being the maximum planning budget and v_{desired} being the desired speed of our UAV. C denotes the exploration weight, and N_{tree} denotes the number of visits to the tree root node while N_{node} denotes the number of times the present node has been visited.

After selecting a candidate node, if it has been visited before, it is expanded by applying motion primitives to generate child nodes, growing the tree. Unvisited nodes skip this step. Following expansion, either the unvisited candidate node or one of its children is selected for the simulation phase, where the future values of nodes along the path are estimated to update the total potential information gain. This informs the selection policy in subsequent iterations. Once planning time is exhausted, the path with the highest information gain is returned.

While MCTS is probabilistically guaranteed to converge to the optimal path [43], it is constrained to actions within a predefined set of motion primitives. Its reliance on random sampling to estimate the future value of nodes can result in poor approximations, particularly in environments with sparse, localized pockets of high information gain. This limitation is especially pronounced in large search areas or scenarios with large budgets constraints, where estimating future node values becomes increasingly expensive. As a result, in such scenarios, MCTS is often implemented with a finite planning horizon, which can restrict its ability to account for long-term consequences or dependencies in the environment.

2) *Greedy*: For the greedy planner, we iterated through each cell within the search bounds and calculated the reward for a given cell i as $g_i = R(X_i)/d_i$ where $R(X_i)$ is given through (2) and d_i represents the Euclidean distance between

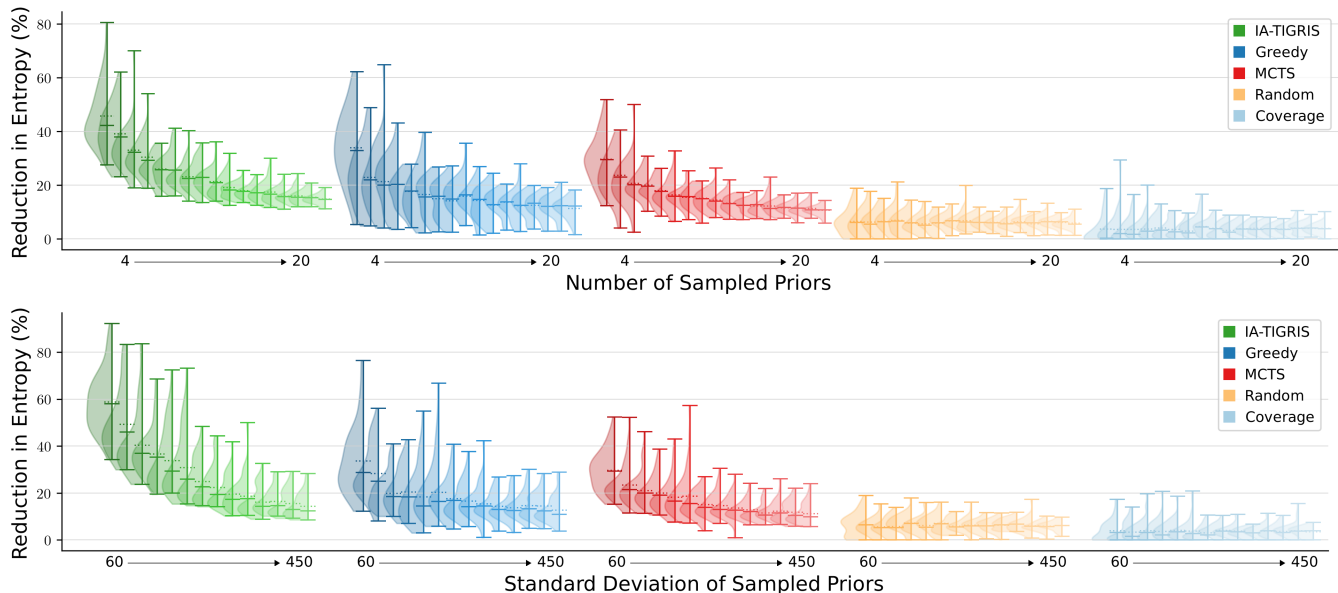


Fig. 13. A comparison of the methods based on the number of sampled prior clusters and the standard deviation of sampled prior clusters. IA-TIGRIS is most effective compared to the baselines when there is high variation in the search space. As the search space prior information becomes more evenly spread out, the performance gap between the methods tends to decrease.

the current position the robot at the current time t and the closest viewpoint to the cell. To compute this viewpoint, the yaw between the current pose of the robot and the intersected cell is first calculated. Using the robot’s sensor configuration and this yaw, x and y coordinates are calculated that view the cell at the desired flight altitude. With this formulation, the planner prioritizes regions with a high ratio of entropy to distance. This can lead to locally optimal choices that contradict with paths that lead to higher information gain over the entire trajectory.

3) *Random*: The random planner operates by iteratively sampling points within the defined search bounds and calculating the minimum-cost path to observe each sampled point. This process is repeated until the available budget is fully expended. The random planner does not utilize any prior information about the environment or target distribution. Additionally, it does not optimize the sequence of actions, instead treating each sampled point independently without considering the global structure of the search problem. This simplicity allows the random planner to highlight the performance benefits of more sophisticated methods by providing a lower-bound comparison for evaluation.

4) *Coverage*: The coverage planner generates a plan that systematically covers the entire search space using a straight-forward lawn-mower pattern. The spacing between each pass is set to match the width of the projected observation footprint at 20% from the bottom, ensuring that no grid cells are missed. This spacing also maintains a distance that enables high-quality sensor measurements. However, due to the size of the search spaces considered, the coverage planner spends significant time surveying empty regions. This approach results in inefficient use of the budget, as it prioritizes full coverage with safe sensor overlap, even in areas with little or no valuable information. While simple and robust, this

method highlights the tradeoff between exhaustive coverage and efficient, targeted exploration.

E. Tests and Analysis

To evaluate the efficacy of IA-TIGRIS against baseline methods, we perform Monte Carlo testing and analyze the impact of the prior and budget on the performance of each method. In all test cases, rewards are calculated using (2), and horizon lengths are set to match the full budget. The tests are conducted on an Intel Xeon CPU E5-2620 v4 @ 2.10GHz, ensuring consistent computational conditions across all evaluations.

1) *Monte Carlo Testing*: Our simulated testing environment is a 5000×5000 m square with Gaussian-distributed prior information randomly placed throughout the search space. The number of prior clusters was sampled uniformly between $[4, 20]$, with standard deviations between $[60, 450]$, and maximum value between $[0.05, 0.5]$.

The results of 100 Monte Carlo tests are shown in Fig. 12. IA-TIGRIS clearly outperforms the other methods, achieving nearly a 40% greater reduction in entropy than the next best method. Early in the simulation, the greedy method initially gains information more quickly, as expected, but this does not translate to better long-term performance. Since our method optimizes for total information gain, it generates paths that maximize information collection over the entire budget. MCTS performed slightly worse than the greedy approach.

The random paths slightly outperformed the coverage paths. This is likely because the lawnmower strategy requires sufficient overlap between passes to avoid missing areas, and its long straight paths often lead to redundant observations due to the UAV’s forward-facing camera. Changing the heading of the UAV is beneficial to viewing more of the search space, which may explain why random paths performed better.

	5000 m	10000 m	15000 m	30000 m	60000 m
IA-TIGRIS	9.41 ± 1.0	18.28 ± 1.8	25.36 ± 2.3	41.08 ± 2.9	58.85 ± 2.9
Greedy	6.99 ± 0.8	13.10 ± 1.5	17.97 ± 2.0	30.00 ± 2.3	49.38 ± 3.5
MCTS	6.06 ± 0.7	11.80 ± 1.1	17.11 ± 1.4	30.21 ± 2.2	48.68 ± 2.7
Random	2.19 ± 0.3	4.29 ± 0.7	6.61 ± 0.6	17.50 ± 1.2	22.47 ± 1.4
Coverage	1.58 ± 0.3	2.82 ± 0.4	4.09 ± 0.7	12.04 ± 1.9	16.77 ± 2.4

TABLE I. Monte Carlo testing results given different budgets. The values are the average percent reduction in entropy and the 95% confidence bounds. IA-TIGRIS had the best performance for all budgets.

We also conducted Monte Carlo tests where either the number of prior clusters or their standard deviation was held constant to analyze how variations in the information map affect planner performance. The results, shown in Fig. 13, include two cases: the upper figure fixes the number of priors, while the lower figure fixes their standard deviation. All other agent and simulation parameters remained unchanged.

Across these tests, the performance gap between IA-TIGRIS and the baselines widens as the number and standard deviation of the Gaussian priors decrease. When entropy is more uniformly distributed across the search space, simpler methods perform reasonably well within the given budget. However, when information is concentrated in sparse, distinct regions, longer-horizon planning becomes essential. In such cases, IA-TIGRIS demonstrates a significant advantage by effectively reasoning about the budget and prioritizing high-value regions.

2) *Budget Analysis*: To evaluate the impact of budget constraints on performance, we conducted additional tests beyond our initial Monte Carlo experiments, evaluating budgets of 5000 m, 10000 m, 30000 m, and 60000 m. Table I summarizes the average entropy reduction across these budgets.

IA-TIGRIS consistently achieved the highest entropy reduction across all budget constraints, with a statistically significant margin over alternative methods. Greedy generally ranked second but was slightly outperformed by MCTS at the 30000 m budget level. Greedy and MCTS exhibited comparable performance throughout the tests, with their results closely tracking each other. Consistent with our previous findings, Random and Coverage methods yielded the lowest results.

Among the tested methods, only IA-TIGRIS and MCTS explicitly incorporate budget constraints into their planning algorithms. Notably, at lower budgets (5000 m and 10000 m), these methods achieved higher entropy reduction compared to the equivalent time steps (200 s and 400 s) in the 15000 m budget scenario shown in Fig. 12. This improved performance stems from IA-TIGRIS’s optimization of total path reward under budget constraints, contrasting with the myopic next-best-action approach of the greedy method. The remaining methods—Greedy, Random, and Coverage—maintain consistent behavior regardless of budget constraints, as their planning strategies do not account for resource limitations.

The performance gap between IA-TIGRIS and the next-best method varied with budget size, showing margins of 34.6%, 39.5%, 41.1%, 36.0%, and 19.2% in ascending budget order. This gap widened through the first three budget levels as problem complexity increased, before declining significantly at higher budgets. This performance pattern suggests that implementing a planning horizon could enhance efficiency by limiting tree search depth, enabling the planner to prioritize path quality optimization over exhaustive space exploration.

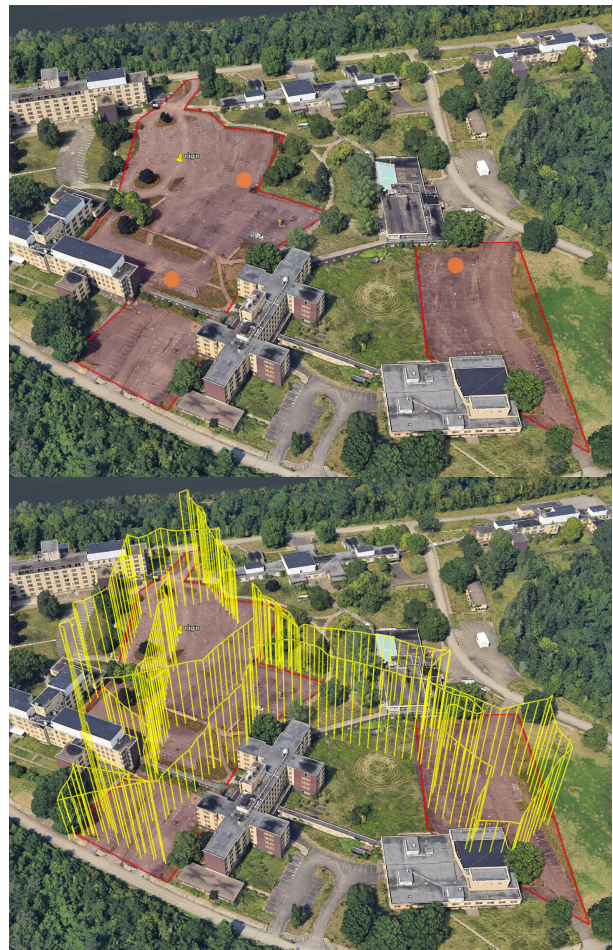


Fig. 14. Google Earth screenshots illustrating the mission planning process and execution. Top: Areas of high entropy targeted for search are highlighted in red, representing regions with a binary occupied/unoccupied probability of 0.2. Three points of particular interest, each assigned a 0.5 probability, are marked in orange. Bottom: The executed drone flight path (yellow) shows the optimized path for maximum information gain across the search space.

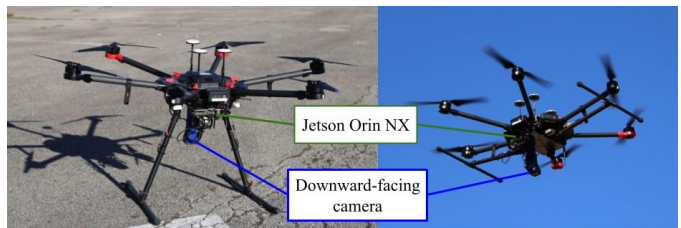


Fig. 15. Hexarotor system (DJI M600 Pro) with onboard compute and camera. Left image shows drone on the ground, right image shows drone in flight.

VI. FIELD DEPLOYMENTS

A. Hexarotor Deployment

The first field experiment that we present uses a hexarotor drone to cover an urban area shown in Fig. 1. We designed this field experiment to simulate classifying where cars are within a search area. Hence, we set the plan request to focus on parking lots at the field test site (Fig. 14, top), with the addition of three chosen grid cells within the parking lots being marked as having a higher uncertainty. The plan request boundaries and priors were created with GPS coordinates in Google Earth,

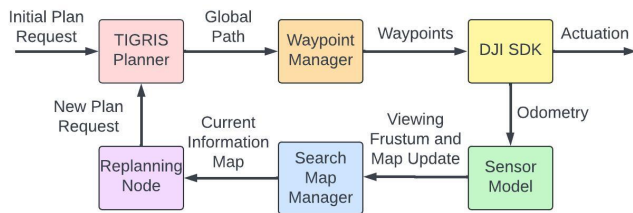


Fig. 16. Functional diagram of the DJI M600 Pro autonomy software.

exported as kml files, and then converted into our plan request message format.

The following sections details the hardware, autonomy, and experimental results for our hexarotor deployments.

1) *Hardware System*: The hardware consists of the DJI M600 Pro, shown in Fig. 15, along with the physical sensing and onboard computer payload. The DJI M600 Pro contains a flight controller that handles pose estimation and position-based control. The DJI M600 Pro’s flight controller also handles teleoperation if human intervention is necessary. Beneath the drone’s base, we mount a custom hardware payload. That payload consists of an onboard computer, a Jetson Xavier, to run the autonomy software shown in Fig. 16. The payload also contains a downward-facing camera for sensing the environment. The camera is a Seek S304SP thermal camera. The camera intrinsics are used to calculate the frustum’s intersection with the search map’s cells in IA-TIGRIS.

2) *Autonomy System*: Fig. 16 illustrates the functional system diagram for the real world field test on the DJI M600. The user specifies the initial plan request prior to takeoff. The TIGRIS planner makes an initial plan on that plan request and sends a global path to the waypoint manager. The waypoint manager tracks the current waypoint within the plan and sends the next waypoint to the DJI software development kit, which then sends actuation commands to the motors. The position of the drone is used to calculate the distance from the drone to the ground and sends that distance parameter to the sensor model. The sensor model’s true positive and false positive rate is used to calculate the per-cell entropy updates in the search map manager. The search map manager publishes the current information map, and the replanning node sends an updated plan request to the IA-TIGRIS planner every ten seconds.

The drone started at an altitude of 50 m above the origin of

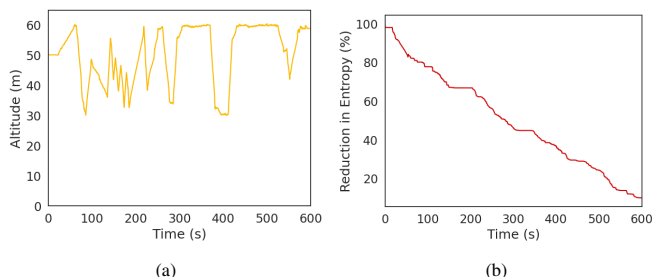


Fig. 17. The results for our hexarotor field deployment. (a) Plot of flown altitude over time, showing large variation throughout the experiment. (b) Reduction in entropy percentage over time of field experiment.



Fig. 18. Fixed-wing platform used for autonomous flights with an onboard camera pitched at 10 degrees [44]

the reference frame. The informed sampler in IA-TIGRIS was set to add states at altitudes of either 30 m or 60 m, creating a trade-off between observation area and detector accuracy. The budget was 2000 m, the planning horizon was 600 m, and the planning time was 10 seconds.

3) *Experimental Results*: The bottom image of Fig. 14 shows the path selected by IA-TIGRIS in the search area. The figure highlights how the planner dynamically adjusts altitudes over time to balance coverage and sensing resolution, maximizing information gain. Higher altitudes allow for broader area coverage, while lower altitudes provide more detailed observations where needed. Additionally, the planner prioritizes revisiting the three regions of higher uncertainty, recognizing the need for repeated observations reduce entropy. This adaptive strategy ensures that uncertain areas receive sufficient attention to improve the belief map. As a result, the entropy of the information map decreases to near zero by the end of the mission, as shown in Fig. 17b, indicating that the planner has effectively gathered the necessary information. This behavior demonstrates the planner’s ability to optimize sensing actions, balancing altitude selection, revisit frequency, and exploration to maximize mission success.

B. Fixed-wing Deployments

Our proposed approach was extensively tested on the fixed-wing AlareTech TL-1 UAV, shown in Fig. 18. The UAV is equipped with an onboard camera pitched at 10 degrees, which introduces a more challenging planning problem due to the non-holonomic motion model and the camera’s field of view. Over more than 20 flight hours and 100 flights running IA-TIGRIS, we validated our approach with the objective to search for objects of interest in a large search space across a variety of test scenarios, including different terrain types, varying environmental conditions, and diverse target distributions. An example mission from these tests is shown in Fig. 19. In this scenario, the planner was given the search bounds and a designated high-priority region. The resulting flight path prioritized revisiting the high-priority area twice, optimizing sensor use and ensuring maximum information gain. This strategy led to the successful detection of the object

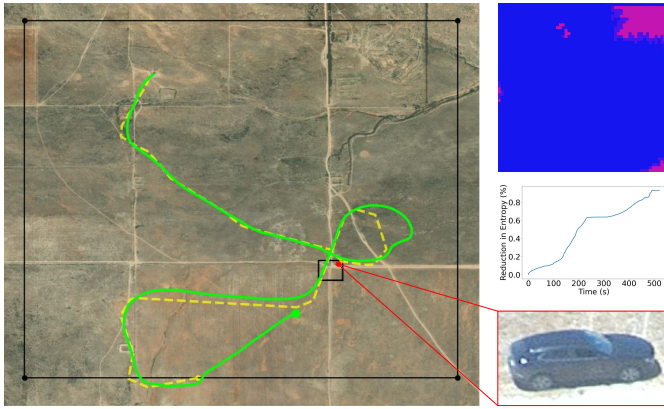


Fig. 19. An example path generated for the fixed-wing platform conducting a large-area search for an object of interest. The larger black rectangle denotes the search bounds, while the smaller black rectangle highlights a region of higher uncertainty. The red dot marks the estimated position of the detected object based on image detections. The upper-right map displays the information state after planning is complete, while the middle plot shows the percent change in entropy over mission time. The flown path illustrates a balance between allocating resources to the high-priority region and exploring other areas within the search space.

of interest, with its estimated position marked by the red dot in the figure.

The map on the upper right in Fig. 19 shows the information map after plan execution was complete. Due to the UAV’s limited budget, the upper right and lower left corners of the map are not searched by the agent. The budget is instead utilized to search over the area of higher priority two times. Compared to the paths in Fig. 14, we observe that the paths for the fixed wing are smoother and have a larger turning radius, demonstrating how IA-TIGRIS respects the motion constraints of the vehicle. We can also see the effect of wind on the path execution, where the flown path shown in green deviates from the planned path shown in yellow. This illustrates the importance of online planning in the cases where this deviation is large or would accumulate over the course of a longer mission and cause the expected observed area to be much different than actual observed area.

VII. CONCLUSION

This paper presents a novel sampling-based IPP planner for autonomous robots that is both adaptive and incremental. Our planner is shown to be effective and computationally efficient, making it suitable for onboard deployment. We conduct a thorough evaluation of individual planner components, providing generalizable insights for other IPP frameworks. Extensive simulation testing against baseline methods highlights the planner’s advantages, and we further validate its effectiveness through demonstrations on two robotic platforms.

Future work includes extending this approach to multi-agent deployments in semi-urban environments for object search and search-and-rescue operations. Further improvements could involve batch sampling and parallel processing to enhance computational efficiency, automatic parameter and horizon selection based on information map characteristics, and integrating trajectory optimization for smoother paths.

Additionally, expanding the framework to support planning with a gimballed camera would enable more flexible and targeted sensing capabilities.

ACKNOWLEDGMENTS

The authors would like to thank Michael Clark for his support as well as Arjun Chauhan, Kevin Gmelin, Sabrina Shen, Manuj Trehan, and Akshay Venkatesh for their contributions in designing the M600 platform.

REFERENCES

- [1] K. Shah, G. Ballard, A. Schmidt, and M. Schwager, “Multidrone aerial surveys of penguin colonies in antarctica,” *Science Robotics*, vol. 5, no. 47, p. eabc3000, 2020.
- [2] S. McCammon and G. A. Hollinger, “Topological path planning for autonomous information gathering,” *Autonomous Robots*, vol. 45, p. 821–842, Sept. 2021.
- [3] D. R. A. De Almeida, E. N. Broadbent, M. P. Ferreira, P. Meli, A. M. A. Zambrano, E. B. Gorgens, A. F. Resende, C. T. de Almeida, C. H. Do Amaral, A. P. Dalla Corte, *et al.*, “Monitoring restored tropical forest diversity and structure through uav-borne hyperspectral and lidar fusion,” *Remote Sensing of Environment*, vol. 264, p. 112582, 2021.
- [4] V. Kaufmann, A. Kellerer-Pirklbauer, and G. Seier, “Conventional and uav-based aerial surveys for long-term monitoring (1954–2020) of a highly active rock glacier in austria,” *Frontiers in Remote Sensing*, vol. 2, p. 732744, 2021.
- [5] J. Lim, N. Lawrance, F. Achermann, T. Stastny, R. Bähmann, and R. Siegwart, “Fisher information based active planning for aerial photogrammetry,” in *2023 IEEE International Conference on Robotics and Automation (ICRA)*, pp. 1249–1255, 2023.
- [6] J. G. A. Barbedo, “A review on the use of unmanned aerial vehicles and imaging sensors for monitoring and assessing plant stresses,” *Drones*, vol. 3, no. 2, p. 40, 2019.
- [7] B. R. Christensen, “Use of uav or remotely piloted aircraft and forward-looking infrared in forest, rural and wildland fire management: evaluation using simple economic analysis,” *New Zealand Journal of Forestry Science*, vol. 45, Sept. 2015.
- [8] J. Patrikar, B. Moon, and S. Scherer, “Wind and the city: Utilizing UAV-based in-situ measurements for estimating urban wind fields,” in *IEEE/RSJ International Conference on Intelligent Robots and Systems (IROS)*, pp. 1254 – 1260, October 2020.
- [9] A. Bashyam and J. W. Guggenheim, “Uavs for wilderness search and rescue: Real-world considerations and technology roadmap for fixed wing uavs,” *The Journal of Search and Rescue*, 2019.
- [10] S. H. Alsamhi, A. V. Shvetsov, S. Kumar, S. V. Shvetsova, M. A. Alhartomi, A. Hawbani, N. S. Rajput, S. Srivastava, A. Saif, and V. O. Nyangaresi, “Uav computing-assisted search and rescue mission framework for disaster and harsh environment mitigation,” *Drones*, vol. 6, p. 154, June 2022.
- [11] M. B. Bejiga, A. Zeggada, A. Nouffidj, and F. Melgani, “A convolutional neural network approach for assisting avalanche search and rescue operations with uav imagery,” *Remote Sensing*, vol. 9, no. 2, p. 100, 2017.
- [12] S. A. H. Mohsan, N. Q. H. Othman, Y. Li, M. H. Alsharif, and M. A. Khan, “Unmanned aerial vehicles (uavs): practical aspects, applications, open challenges, security issues, and future trends,” *Intelligent Service Robotics*, Jan. 2023.
- [13] R. Bailon-Ruiz, A. Bit-Monnot, and S. Lacroix, “Real-time wildfire monitoring with a fleet of uavs,” *Robotics and Autonomous Systems*, vol. 152, p. 104071, 2022.
- [14] M. Dunbabin and L. Marques, “Robots for environmental monitoring: Significant advancements and applications,” *IEEE Robotics & Automation Magazine*, vol. 19, no. 1, pp. 24–39, 2012.
- [15] A. Singh, A. Krause, C. Guestrin, and W. J. Kaiser, “Efficient informative sensing using multiple robots,” *Journal of Artificial Intelligence Research*, vol. 34, p. 707–755, Apr 2009.
- [16] L. Bottarelli, M. Bicego, J. Blum, and A. Farinelli, “Orienteering-based informative path planning for environmental monitoring,” in *Engineering Applications of Artificial Intelligence*, vol. 77, pp. 46–58, 2019.
- [17] S. Arora and S. Scherer, “Randomized algorithm for informative path planning with budget constraints,” in *2017 IEEE International Conference on Robotics and Automation (ICRA)*, (Singapore, Singapore), pp. 4997–5004, IEEE, May 2017.

- [18] A. Singh, A. Krause, C. Guestrin, and W. Kaiser, "Efficient informative sensing using multiple robots," *J. Artif. Intell. Res. (JAIR)*, vol. 34, pp. 707–755, 01 2009.
- [19] A. Meliou, A. Krause, C. Guestrin, and J. M. Hellerstein, "Nonmyopic informative path planning in spatio-temporal models," in *Proceedings of the 22nd National Conference on Artificial Intelligence - Volume 1, AAAI'07*, p. 602–607, AAAI Press, 2007.
- [20] C. Chekuri and M. Pal, "A recursive greedy algorithm for walks in directed graphs," in *Proceedings of the 46th Annual IEEE Symposium on Foundations of Computer Science, FOCS '05*, (USA), p. 245–253, IEEE Computer Society, 2005.
- [21] H. Cheng, Z. Yang, and C. Chan, "An expert system for decision support of municipal water pollution control," *Engineering Applications of Artificial Intelligence*, vol. 16, pp. 159–166, 03 2003.
- [22] S. Pang and J. Farrell, "Chemical plume source localization," *IEEE Transactions on Systems, Man, and Cybernetics, Part B (Cybernetics)*, vol. 36, no. 5, pp. 1068–1080, 2006.
- [23] A. Singh, A. Krause, C. Guestrin, and W. J. Kaiser, "Efficient informative sensing using multiple robots," in *CoRR*, vol. abs/1401.3462, 2014.
- [24] P. Vansteenwegen, W. Souffriau, and D. V. Oudheusden, "The orienteering problem: A survey," *European Journal of Operational Research*, vol. 209, p. 1–10, Feb. 2011.
- [25] A. Jones, M. Schwager, and C. Belta, "A receding horizon algorithm for informative path planning with temporal logic constraints," in *2013 IEEE International Conference on Robotics and Automation*, pp. 5019–5024, 2013.
- [26] W. Sun, N. Sood, D. Dey, G. Ranade, S. Prakash, and A. Kapoor, "No-regret replanning under uncertainty," in *2017 IEEE International Conference on Robotics and Automation (ICRA)*, pp. 6420–6427, 2017.
- [27] S.-H. Yoo, A. Stuntz, Y. Zhang, R. Rothschild, G. A. Hollinger, and R. N. Smith, *Experimental Analysis of Receding Horizon Planning Algorithms for Marine Monitoring*, p. 31–44. Springer International Publishing, 2016.
- [28] S. Kailas, "Multi-robot information gathering for spatiotemporal environment modelling," Master's thesis, Carnegie Mellon University, Pittsburgh, PA, August 2023.
- [29] S. Frolov, B. Garau, and J. Bellingham, "Can we do better than the grid survey: Optimal synoptic surveys in presence of variable uncertainty and decorrelation scales," *Journal of Geophysical Research: Oceans*, vol. 119, no. 8, pp. 5071–5090, 2014.
- [30] B. Moon, S. Chatterjee, and S. Scherer, "Tigris: An informed sampling-based algorithm for informative path planning," in *IEEE/RSJ International Conference on Intelligent Robots and Systems (IROS)*, 2022.
- [31] J. Binney and G. S. Sukhatme, "Branch and bound for informative path planning," in *2012 IEEE International Conference on Robotics and Automation*, pp. 2147–2154, 2012.
- [32] G. Best and R. Fitch, "Probabilistic maximum set cover with path constraints for informative path planning," in *Australasian Conference on Robotics and Automation*, ARAA, 12 2016.
- [33] C. E. Rasmussen and C. K. I. Williams, *Gaussian Processes for Machine Learning*. The MIT Press, 2006.
- [34] G. A. Hollinger and G. S. Sukhatme, "Sampling-based robotic information gathering algorithms," *The International Journal of Robotics Research*, vol. 33, p. 1271–1287, June 2014.
- [35] L. Schmid, M. Pantic, R. Khanna, L. Ott, R. Siegart, and J. Nieto, "An Efficient Sampling-Based Method for Online Informative Path Planning in Unknown Environments," *IEEE Robotics and Automation Letters*, vol. 5, pp. 1500–1507, Apr. 2020.
- [36] G. Hollinger, "Long-horizon Robotic Search and Classification using Sampling-based Motion Planning," in *Robotics: Science and Systems XI*, Robotics: Science and Systems Foundation, July 2015.
- [37] A. Arora, P. M. Furlong, R. Fitch, S. Sukkarieh, and T. Fong, "Multi-modal active perception for information gathering in science missions," *Autonomous Robots*, 10 2019.
- [38] J. Das, J. Harvey, F. Py, H. Vathsangam, R. Graham, K. Rajan, and G. S. Sukhatme, "Hierarchical probabilistic regression for auv-based adaptive sampling of marine phenomena," in *2013 IEEE International Conference on Robotics and Automation*, p. 5571–5578, IEEE, May 2013.
- [39] K.-C. Ma, L. Liu, H. Heidarsson, and G. Sukhatme, "Data-driven learning and planning for environmental sampling," *Journal of Field Robotics*, vol. 35, 02 2017.
- [40] R. Marchant and F. Ramos, "Bayesian optimisation for informative continuous path planning," in *2014 IEEE International Conference on Robotics and Automation (ICRA)*, pp. 6136–6143, 2014.
- [41] A. Bender, S. B. Williams, and O. Pizarro, "Autonomous exploration of large-scale benthic environments," in *2013 IEEE International Conference on Robotics and Automation*, pp. 390–396, 2013.
- [42] Google, "Benchmark." <https://github.com/google/benchmark>, 2024.
- [43] T. Dam, G. Chalvatzaki, J. Peters, and J. Pajarinen, "Monte-carlo robot path planning," *IEEE Robotics and Automation Letters*, vol. 7, no. 4, pp. 11213–11220, 2022.
- [44] A. Technologies, "What we do." <https://alaretech.com/capabilities.html>, 2022. [Accessed: 15 December 2024].